PHYSICAL REVIEW LETTERS

Structural Polymorphism of the Actin-Espin System: A Prototypical System of Filaments and Linkers in Stereocilia

Kirstin R. Purdy,[1] James R. Bartles,[2] and Gerard C. L. Wong[1]

[1]*Department of Materials Science and Engineering, University of Illinois at Urbana-Champaign, Urbana, Illinois 61801, USA*
[2]*Department of Cell and Molecular Biology, Northwestern University, Feinberg School of Medicine, Chicago, Illinois 60611, USA*
(Received 30 June 2006; published 1 February 2007)

We examine the interaction between cytoskeletal F-actin and espin 3A, a prototypical actin bundling protein found in sensory cell microvilli, including ear cell stereocilia. Espin induces twist distortions in F-actin as well as facilitates bundle formation. Mutations in one of the two F-actin binding sites of espin, which have been implicated in deafness, can tune espin-actin interactions and radically transform the system's phase behavior. These results are compared to recent theoretical work on the general phase behavior linker-rod systems.

The cytoskeletal organization of filamentous actin (F-actin), a biological rodlike polyelectrolyte, is controlled predominantly by actin binding proteins (ABPs), which cross-link actin into a polymorphism of bundle and network phases [1–3], through a process that has recently been examined theoretically [4,5]. Espins are a recently discovered class of ABPs responsible for the formation of parallel actin bundles *in vivo* and *in vitro* [6–8]. A specific isoform, espin 3A, is found in actin bundles in sensory cell microvilli, such as the stereocilia of cochlear hair cells, which are vital for the transduction of sound in hearing [9–11]. Genetic mutations in espin's F-actin binding sites are linked to malformed stereocilia, deafness, and vestibular dysfunction in humans and mice [11–13]. Such "deafness" mutations allow us to assess the role of linker "stickiness" in the organization of actin bundles.

In this Letter we describe the first measurements of self-assembled espin-actin bundle structure, and show how interactions between F-actin and different espin linkers are expressed in the system's phase behavior. Small angle x-ray scattering (SAXS) shows that as espin concentration increases, the system evolves directly from an isotropic phase to hexagonally coordinated paracrystalline bundles of hypertwisted filaments. As the ability of a given espin to cross-link F-actin is decreased by using two different genetically modified deafness mutants of espin with progressively more severe damage to one of the two actin binding sites, an unanticipated nematic actin-espin network is observed. By mixing wild type (wt) and mutant espin, which allows us to continuously tune this cross-linking affinity between espin and actin, we find that the onset of this nematic-network phase is a strong function of espin cross-linking affinity and concentration. This unexpected isotropic to nematic network transition has strong implications for stereocilia formation and hearing.

F-actin was prepared from lyophilized rabbit skeletal muscle G-actin monomer (42 kDa, Cytoskeleton, Inc). G-actin was resuspended in 5 mM tris, with 0.2 mM CaCl$_2$, 0.5 mM ATP, 0.2 mM dithreithol (DTT) and 0.01% NaN$_3$ at pH 8.0 and polymerized into F-actin upon the addition of 100 mM KCl. F-actin is treated with human plasma gelsolin (Cytoskeleton, Inc.) to control average length (~1 μm) and with phalloidin to prevent depolymerization. F-actin was then pelleted at 100 000g and resuspended overnight in E-buffer: 0.1 M KCl, 10 mM HEPES, 1 mM DTT, 1.5 mM NaN$_3$, pH 7.4.

Four espin proteins were expressed recombinantly in bacteria with an N-terminal 6x His tag (3.4 kDa), purified under nondenaturing conditions and suspended in E-buffer [6,7]: 30.9 kDa wt rat espin 3A, rE3A (GenBank AY587568); 30.9 kDa wt human espin 3A, hE3A; 30.9-kDa human espin 3A with the 2541-2543delAAG mutation [13], hE3AdelK; and 29.8 kDa human espin 3A with the 2469delGTCA mutation [12], hE3AdelCt. Espin's carboxy (C)-terminal peptide, which is necessary and sufficient for F-actin bundling, contains two F-actin binding sites [6]. HE3AdelK is associated with dominant deafness and results in the loss of a single lysine residue from the F-actin binding site closest to the C-terminus [13]. HE3AdelCt is associated with recessive deafness and causes a frameshift that replaces the 31 C-terminal amino acids with an unrelated 21-amino acid peptide thereby eliminating the C-terminal F-actin-binding site [12]. Espin is thought to be an anisotropic protein with a Stokes radius of 3.4 nm [6], though the tertiary structure is still unknown.

Solutions of F-actin at 3.75 mg/ml and espin at specific molar ratios $\rho = N_{\text{espin}}/N_{G\text{-actin}}$ were mixed and sealed in 1.5 mm quartz capillaries (Charles Supper Co., MA), incubated at room temperature for 1 h, and finally centrifuged at 9000g for 2 h to sediment the F-actin-espin complexes. This actin concentration (3.75 mg/ml) is much lower than the measured isotropic-nematic (I-N) transition concentration (>7 mg/ml) for 1 μm F-actin under similar ionic conditions [14]. SAXS experiments were performed both at 9 KeV at BL4-2 of the Stanford Synchrotron Radiation Laboratory and at 12 KeV the BESSRC-CAT (BL12-ID) at the Advanced Photon Source. The scattered radiation was collected using a

MAR Research charge-coupled device camera (pixel size = 79 μm) at both beam lines. Capillaries were also imaged under cross polarizers to check for birefringence of the espin/actin suspensions. In the absence of espin linkers, the F-actin is isotropically oriented and appears dark under crossed polarizers.

Figure 1(a) shows typical circularly averaged SAXS data from rE3A-actin bundles. The sharp Gaussian peaks indicate that espin-actin mixtures form hexagonally coordinated bundles over a wide range of ρ. The maximum espin packing within actin bundles is 1 linker for 3–4 actin monomers ($\rho = 0.3$–0.4), similar to that for most bundle-forming linker proteins [6,7]. Interestingly, the espin-actin bundle structure persists down to $\rho = 0.02$ (for both the rE3A-actin bundles [Fig. 1(a)] and hE3A-actin bundles [Fig. 3(a)], but with an increasing fraction of coexisting unbundled, isotropic, F-actin with decreasing ρ. This suggests that espin is not homogeneously distributed but instead segregates to bundles. At $\rho = 0.02$ broad $-13/6$ layer lines from the native untwisted state of individual actin filaments are visible coexisting with sharp Gaussian layer-line peaks from actin bundle organization. For comparison, physiological ρ is approximately $0.07 - 0.05$ in Sertoli cell parallel actin bundles [7] and in stereocilia [15].

Figure 1(b) is a 2D diffraction pattern for partially aligned espin-actin bundles at $\rho = 0.2$. Angularly aver-

aged wedges of intensity along q_r and q_z are shown in Figs. 1(d) and 1(e). The index diffraction peaks along q_r unambiguously indicate hexagonal F-actin packing, with peak positions corresponding to hexagonal reciprocal lattice vectors of q_{10}, $q_{01} = \sqrt{3}q_{10}$, $q_{20} = 2q_{10}$, $q_{21} = \sqrt{7}q_{10}$, $q_{30} = 3q_{10}$, $q_{12} = \sqrt{8}q_{10}$, $q_{22} = 2\sqrt{3}q_{10}$. The measured inter-actin spacing of $4\pi/\sqrt{3}q_{10}$ is equal to 12.6 ± 0.2 nm and corresponds to a surface-to-surface distance of ~ 5.1 nm, assuming an F-actin diameter of 7.5 nm.

Along q_z the intrafilament diffraction from the F-actin rods is visible as three Gaussian-shaped peaks at 0.120, 0.135, and 0.146 Å^{-1}. These peaks originate from the convolution of the helical F-actin structure and the hexagonal bundle structure [16]. For unbundled F-actin, the characteristic 6th and 7th layer line diffraction from the F-actin form factor, $F(q)$, ($-13/6$ monomers/turn symmetry) can be observed as peaks at 0.114 and 0.125 Å^{-1} when angularly averaged [$\rho = 0.02$ in Fig. 1(a)]. However, because of the paracrystalline hexagonal coordination of the bundles, the 2D F-actin layer-line pattern is visible only as a series of strong spots aligned along q_z in columns at q_r values corresponding to the hexagonal reciprocal lattice vector $S(q)$ [Fig. 2(a)]. By fitting the experimental results to calculated diffraction curves from model F-actin with arbitrary degrees of overtwisting [2,17], we found that the F-actin in the espin induced bundles was overtwisted by $0.9° \pm 0.2°$ from the $-13/6$, or -2.167, monomers/turn twist to a value of -2.154 ± 0.004 monomers/turn with a G-actin monomer spacing of 27.6 Å in the rE3A induced bundles. In the model diffraction pattern, $F(q)$ was calculated using the 4-sphere model for the G-actin monomer [2,17] and $S(q)$ was modeled as a Gaussian centered at the first peak in the hexagonal reciprocal lattice, $S(q_r) = \exp[-\pi(q_r - 0.0575)^2/\sigma^2]$, such that the intensity, $I(q) = S(q)F(q)$. A representative fit to the data in Fig. 1(e) is shown in Fig. 2(b). This overtwisting suggests a significant degree of intra-actin torsional strain within espin-actin bundles. Interestingly, the espin induced twist is larger than the measured twist for both stereocilia bundles *in vitro*
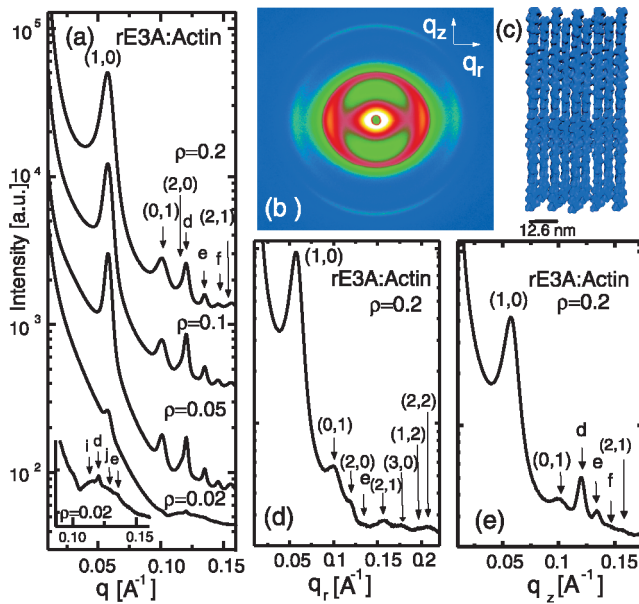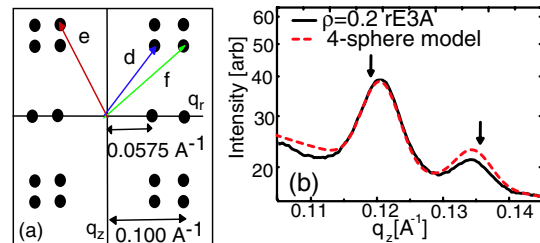

FIG. 1 (color). (a) Circularly averaged diffraction from rE3A-actin mixtures at different ρ showing hexagonally indexed peaks and layer line peaks. (b) Partially aligned 2D diffraction pattern of rE3A-actin bundles at $\rho = 0.2$. (c) Proposed espin-actin bundle structure; espin linkers are omitted for clarity. Angularly averaged wedges along the radial (q_r) and axial (q_z) directions of (b) are shown in (d) and (e). Labeled layer line diffraction peaks are (d) 0.120, (e) 0.135, and (f) 0.146 Å^{-1}. Inset in (a) shows coexisting bundled and unbundled F-actin layer line peaks (i) 0.114 and (j) 0.124 Å^{-1} for $\rho = 0.02$.

FIG. 2 (color online). (a) Model 2D diffraction pattern of a near-crystalline hexagonally ordered rE3A-actin bundle aligned parallel to q_z. Horizontal layer lines are only visible at q_r values where $S(q)$ is nonzero. The peaks labeled d, e, and f correspond to the peaks in Fig. 1(e). (b) Fit to the intrahelical diffraction peaks from Fig. 1(e) using the 4-sphere G-actin model multiplied by $S(q)$. Arrows indicate corresponding peak positions of $-13/6$ native actin twist symmetry.

(−2.159) and bundles generated with fimbrin (−2.160), an ABP which is also found in stereocilia [16,18], suggesting that the espins may be strained in stereocilia. A similar analysis of hE3A-actin bundles reveals that the bundle structure is identical, independent of species (rat vs human). Circularly averaged diffraction for hE3A-actin bundles is presented in Fig. 3(c). The layer-line fitting for the hE3A returns an overtwist of $1.0° ± 0.2°$ and monomer spacing of 27.6 Å. This columnar hexagonal lattice of uniformly twisted filaments [Fig. 1(c)] is significantly more ordered than other F-actin bundles previously studied in solution, including α-actinin-actin bundles [3] and close-packed, multivalent ion mediated actin bundles [2].

By replacing the wt espin with one of the espin mutants we found a drastically different phase behavior with changing ρ. Unlike hE3A, the single amino acid deletion mutant hE3AdelK only bundles actin at high ρ [Fig. 3(d)], and the resultant bundles have a larger and more variable inter-actin spacing (12.6 to 14.6 nm). With decreasing ρ the bundle peak decreases in intensity and an unexpected broad correlation peak appears at $q_n \sim 0.025$ Å^{-1}, which displays a 2D "bow-tie" pattern characteristic of nematics [Fig. 3(a)]. This suggests that small concentrations of hE3AdelK induce spontaneous orientation in the isotropic F-actin but with only short-range positional ordering, in contrast to the highly ordered bundles made with hE3A at similar ρ [Fig. 3(c)]. The inter-actin spacing of this nematiclike structure, $2\pi/q_n$, is about $19 ± 1.5$ nm, as illustrated in Fig. 3(b). This observed inter-actin spacing is striking because such a short spacing is observed in a linker-free nematic only if the F-actin concentration is increased to about 70 mg/ml [dashed curve in Fig. 3(e)], at which point it also exhibits much sharper nematic peaks. This suggests that the observed phase is a weakly ordered, partially cross-linked, nematic network (NN). We note that
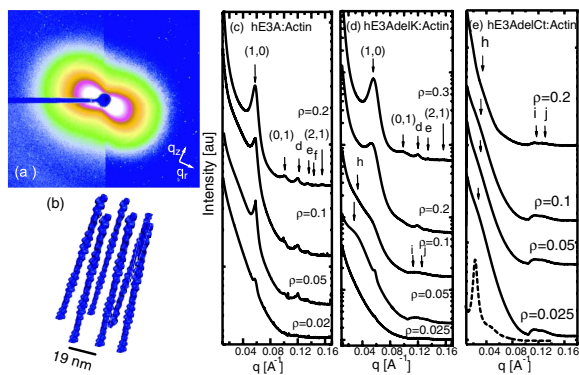
under crossed polarizers, these NN samples were birefringent with multiple domain orientations, suggesting that the nematic pattern was not induced by the centrifugation during sample preparation [15]. Also, this NN phase did not sediment upon centrifugation, indicating that the density is similar to that of the buffer, unlike bundles [6]. A similar NN peak with an even larger inter-actin spacing of $21.3 ± 2.5$ nm is observed for all ρ in mixtures using the most damaged espin mutant hE3AdelCt [Fig. 3(e)]. Unlike the hE3AdelK:actin mixtures, no bundle peaks are observed in the hE3AdelCt:actin suspensions. This suggests that as the severity of the espin mutation increases, the actin cross-linking affinity of the espin decreases and the inter-actin spacing increases. Furthermore, the twist of the actin in the NN phase induced by both mutant espins is equal to the native twist of $-13/6$ monomers/turn, suggesting that the mutant espins are not strong enough to maintain the twisted intrabundle coordination.

Fluorescence microscopy reveals condensed aggregates for both hE3A-actin and hE3AdelK-actin mixtures (Fig. 4). From the SAXS data, the phase of the hE3AdelK-actin mixture in Fig. 4(b) ($\rho = 0.06$) is predominantly in the NN phase, whereas the hE3A-actin mixture in Fig. 4(a) ($\rho = 0.2$) is predominantly in the bundle phase. With increasing ρ, the number of observed hE3A-actin aggregates increases, and the proportion of isotropic F-actin decreases [compare Figs. 4(a) and 4(c)]. The number of aggregates for hE3AdelK-actin at similar ρ is also less than the hE3A-actin mixtures. The observation of similar aggregates in hE3A-actin and hE3AdelK-actin mixtures is consistent with the similar inter-actin spacings of the bundle and NN phases determined from SAXS data, although microscopy did not reveal their drastic difference in internal ordering. The hE3AdelK-actin aggregates in Fig. 4(b) are also consistent with the observation of hexagonal bundles in Fig. 3(d). However, the aggregates in the hE3AdelK-actin mixtures may also be disordered bundle structures, similar to those observed for microtubules condensed with low valence counterions [19], as the diffraction data suggests that hE3A-actin and hE3AdelK-actin organizations are quite different. This similarity to Ref. [19] is consonant with the hypothesized homology between the role of linkers and multivalent ions in rodlike polyelectrolyte organization [5,20].

Theoretical work on rigid polyelectrolytes and linkers predicts that changing linker properties induces an isotropic network to bundle transition [5], but does not vary the cross-linking affinity of the linkers, as in our experiments. The NN to bundle transition we observe with increasing cross-linking affinity of the espin (by switching from mutant espin to wt espin) is analogous to the isotropic network to bundle transition predicted for different linkers, however, the isotropic to NN transition observed with increasing weak-linker concentration is a qualitatively new feature of these systems. The nematic orientation is only predicted to depend on rod concentration (via an I-N transition). Interestingly, simulations of polyelectrolyte chains
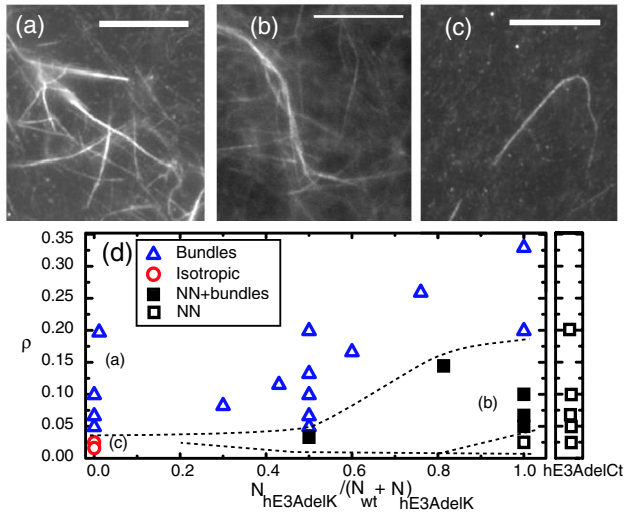

FIG. 3 (color online). (a) 2D diffraction pattern from a NN suspension of actin-hE3AdelK at $\rho = 0.05$. (b) Proposed actin-hE3AdelK NN structure oriented with (a); espin linkers are omitted for clarity. Circularly averaged diffraction intensities for suspensions of F-actin mixed with hE3A, hE3AdelK, and hE3AdelCt are shown in (c), (d) and (e), respectively. Dashed curve in (f) is nematic F-actin at 70 mg/ml. Labeled diffraction peaks d, e, f, i, and j are the same as those in Fig. 1. The broad feature at h is the nematic correlation, $q_n = 0.024$–0.026 Å^{-1}.

FIG. 4 (color online). Fluorescence microscopy images of 0.5 g/L, 10 μm F-actin (a) bundled with hE3A at $\rho = 0.2$, (b) condensed with hE3AdelK at $\rho = 0.06$, (c) coexisting with bundles of hE3A-actin at $\rho = 0.03$. Alexa546-phalloidin dyed F-actin concentration is fixed at 0.03 g/L. Coexisting isotropic F-actin in (b) and (c) are visible as faint gray lines. Scale bar is 10 μm. (d) Phase diagram of espin-actin complexes determined from the SAXS data showing predominant phases as a function of ρ and different ratios of hE3A and hE3AdelK. On the far right, the hE3AdelCt-actin phase behavior is included. The location of images (a), (b), and (c) are also indicated in (d). All phases include some isotropic F-actin. Dashed lines estimate the phase boundaries.

with weak linkers suggest that they can induce end-on overlapping of the charged rods, instead of complete bundle formation [4]. This end-on overlapping effectively increases the average rod length (L), and could consequently induce an I-N transition, as illustrated by Onsager's equation for the nematic coexistence concentration of charged rods: $n = 18/\pi L^2 D_{eff}$ [21], where D_{eff} is the effective hard rod diameter of a charged rod. Shear alignment in the presence of linkers may also contribute to NN formation during sample mixing. However, the same shear forces are present for all samples including isotropic and bundled phases. Both end-on and non-end-on cross-linking may contribute to our observation of an isotropic to NN transition in the presence of weak linkers (hE3AdelK, hE3AdelCt).

The SAXS data are summarized in an espin-actin phase diagram as a function of ρ and average espin cross-linking affinity [Fig. 4(d)]. By varying the ratio of hE3AdelK to hE3A we tune the effective cross-linking affinity of the espin in a continuous manner. This measurement of mixed wt and mutant espin is important biologically, as only heterozygous hE3AdelK expression has been observed in humans [13]. As the cross-linking affinity of the linkers decreases the NN becomes stable at higher ρ. In fact, the NN phase dominates the phase diagram for the weakest

espin linker, hE3AdelCt (far right panel). It would be interesting to see if this tendency to form a NN from an isotropic rod suspension can be captured by a variation of the linker cross-linking affinity [5].

We have shown that structure of espin-actin complexes changes drastically when the wt espin is replaced with deafness mutants, from cross-linked parallel hexagonal actin bundles (like those found in cochlear hair cell stereocilia), to a previously unanticipated NN phase. Increasing the damage to one of the actin binding sites (by switching from hE3AdelK to hE3AdelCt) further destabilizes the bundle structure and results in a NN phase for all ρ. A NN phase in stereocilia would make a poor mechanical sensor because the different espin linkage and potential for interfilament sliding is expected to decrease the bending modulus by 3 orders of magnitude from that of paracrystalline bundles [1,22].

[1] J. H. Shin *et al.*, J. Mol. Biol. **337**, 255 (2004).
[2] T. E. Angelini *et al.*, Eur. J. Phys. **16**, 389 (2005).
[3] O. Pelletier *et al.*, Phys. Rev. Lett. **91**, 148102 (2003).
[4] I. Borukhov *et al.*, J. Chem. Phys. **117**, 462 (2002).
[5] I. Borukhov *et al.*, Proc. Natl. Acad. Sci. U.S.A. **102**, 3673 (2005).
[6] J. R. Bartles *et al.*, J. Cell Biol. **143**, 107 (1998).
[7] B. Chen *et al.*, Mol. Biol. Cell **10**, 4327 (1999).
[8] G. Sekerkova *et al.*, J. Neurosci. **24**, 5445 (2004).
[9] A. Rzadzinska *et al.*, Cell Motil. Cytoskeleton **62**, 157 (2005).
[10] H. Li *et al.*, J. Comp. Neurol. **468**, 125 (2004).
[11] L. Zheng *et al.*, Cell **102**, 377 (2000).
[12] S. Naz *et al.*, J. Med. Genet. **41**, 591 (2004).
[13] F. Donaudy *et al.*, J. Med. Genet. **43**, 157 (2005).
[14] J. Viamontes, P. W. Oakes, and J. X. Tang, Phys. Rev. Lett. **97**, 118103 (2006).
[15] K. Purdy J. Bartles, and G. C. L. Wong (unpublished).
[16] L. Tilney, D. J. Derosier, and M. J. Mulroy, J. Cell Biol. **86**, 244 (1980).
[17] H. Al-Khayat, N. Yagi, and J. M. Squire, J. Mol. Biol. **252**, 611 (1995).
[18] N. Volkmann *et al.*, J. Cell Biol. **153**, 947 (2001).
[19] D. J. Needleman *et al.*, Proc. Natl. Acad. Sci. U.S.A. **101**, 16 099 (2004).
[20] G. C. L. Wong *et al.*, Phys. Rev. Lett. **91**, 018103 (2003).
[21] L. Onsager, Ann. N.Y. Acad. Sci. **51**, 627 (1949).
[22] G. M. Grason and R. F. Bruinsma, Phys. Rev. Lett. **97**, 027802 (2006).